02,05

Small magnetic hysteresis and anisotropy of textured high-temperature superconductor Bi2223

© D.A. Balaev, S.V. Semenov, D.M. Gokhfeld, M.I. Petrov

Kirensky Institute of Physics, Federal Research Center KSC SB, Russian Academy of Sciences, Krasnoyarsk, Russia

E-mail:dabalaev@iph.krasn.ru

Received June 25, 2025
Revised June 25, 2025
Accepted June 28, 2025

In materials based on high-temperature superconductors (HTSC) with a pronounced granular structure, along with the main superconducting subsystem — HTSC granules, an additional subsystem with weakened superconducting properties appears, formed by intergranular boundaries (Josephson junctions). This „weak" superconducting subsystem manifests itself as a „small" magnetic hysteresis existing in a certain range of sufficiently weak external fields. In this paper, we study the small magnetic hysteresis of a textured sample of $Bi_{1.8}Pb_{0.3}Sr_{1.9}Ca_2Cu_3O_x$ (Bi2223), in which the plate-like Bi2223 crystallites are predominantly oriented relative to the crystallographic c-axis. It is found that the range of existence of a small hysteresis differs for the directions of the external magnetic field **H** parallel and perpendicular to the orientation of the c-axis of the crystallites. To explain this experimental fact, the influence of magnetic moments of Bi2223 crystallites on the effective field in the intercrystallite boundaries is considered. The magnetic induction lines from the magnetic moments of superconducting crystallites are closed through the intercrystallite boundaries, and at the orientation $\mathbf{H} \perp c$ a partial compensation of the field induced by neighboring crystallites occurs due to their misalignment. This leads to the fact that the influence of the main superconducting subsystem (Bi2223 crystallites) on the intercrystallite boundary subsystem is smaller, and the range of the external field in which a small hysteresis exists is larger at $\mathbf{H} \perp c$ than at $\mathbf{H} \parallel c$.

Keywords: textured high-temperature superconductor, Bi2223, magnetic hysteresis.

DOI: 10.61011/PSS.2025.07.61866.156-25

1. Introduction

The type of magnetic hysteresis loop and the absolute values of the magnetization of superconductors of the second kind are determined by the processes of field penetration in the form of Abrikosov vortices, as well as their movement, pinning, and interaction with each other. These processes have been well studied for various superconducting materials. If a material consists of superconducting regions separated by a non-superconducting material, then a network of Josephson junctions is possible in such a material. For this, it is necessary that the size of the non-superconducting interspaces be comparable to the coherence length of the superconductor. In this case, the magnetic hysteresis loop is determined by contributions from the „weak" and „strong" superconducting subsystems: shielding currents flow throughout the sample (both through superconducting regions and through the interspaces between them), and the trapped magnetic flux is formed by Abrikosov vortices and Josephson vortices.

A network of Josephson junctions is usually artificially formed on thin films for low-temperature superconductors with a sufficiently long coherence length [1–3]. For the class of high-temperature superconductors (HTSC), a network of Josephson junctions is formed naturally in materials with pronounced granularity. In this case, the transition region from one granule to another, i. e., the intergranular boundary, has a length of several nanometers, which is comparable to the coherence length of the HTSC.

Studies conducted in the first two decades after the discovery of HTSC [4–12] have shown that the subsystem of intergranular boundaries in granular HTSC manifests itself in magnetic hysteresis as a „small" loop in the region of sufficiently weak fields. This subsystem is characterized by low values of the first penetration field H_{1P} (i. e., of the first critical field) and small values of the field H_{irr1} of irreversible magnetization behavior. For example, for yttrium and bismuth HTSC, typical values of H_{irr1} are $\sim 5-20$ Oe at „nitrogen" temperature (77 K) [4,5,8] and ~ 100 Oe in the vicinity of „helium" temperature (4 K) [7,10–13] (the H_{1P} value is less than the Earth's field at „nitrogen temperature" [14]).

However, it cannot be said that small magnetic hysteresis has been studied in the same detail as the main („large") magnetic hysteresis, which manifests itself in moderate and large fields. The number of papers devoted to small hysteresis is small [4–12]. Particularly, the issue of the interaction of two superconducting subsystems (granules and intergranular boundaries) was not considered in detail in the cited papers. It is clear that the magnetization hysteresis loop is caused by two contributions: from granules and from the subsystem of intergranular boundaries. At the same time, the „weak"

subsystem of intergranular boundaries is generated by the „strong“ subsystem of granules. However, it turned out that the magnetic moments of the granules strongly suppress the subsystem of intergranular boundaries [15–17], and this influence becomes dominant under certain conditions (the external field, the magnetic flux trapped by the granules). In fact, the contribution from the intergranular boundary subsystem is clearly expressed in the general hysteresis loop only in the area of small fields ($\pm H_{\text{irr1}}$), however, after increase of the external field to a certain value, and then decrease of the field, this contribution completely disappears in the same area of small fields ($\pm H_{\text{irr1}}$) [13,15–17].

Small magnetic hysteresis has been studied for the main classes of HTSC systems based on yttrium and bismuth [4–13,15–17]. The case of a textured material with spatially ordered crystallites (hereinafter the terms „crystallite“ and „granule“ are identical) with strong anisotropy of superconducting properties remained unexplored. We studied in this paper a textured sample $Bi_{1.8}Pb_{0.3}Sr_{1.9}Ca_2Cu_3O_x$ (Bi2223), in which The Bi2223 lamellar crystallites are predominantly oriented relative to the crystallographic c-axis. Due to the strong anisotropy of the superconducting properties of individual crystallites, the textured polycrystalline sample has an anisotropy of the main magnetic hysteresis. The aim of the study was to establish and explain the nature of the anisotropy of the small magnetic hysteresis of such a textured superconductor.

2. Experiment

2.1. Method of preparation and results of characterization of a textured sample

The preparation of textured Bi2223 was described earlier [18]. The essence of the method is that at the initial stage, a porous sample with a density of 26−40 % of the theoretical density of Bi2223 is obtained with additives of ultrafine silver. In the resulting porous sample, Bi2223 crystallites have the shape of plates with a thickness of $1-2\,\mu$m and linear dimensions of $\sim 20-30\,\mu$m. The thin part of the plates corresponds to the crystallographic c-axis, and the long sides correspond to the crystallographic $a-b$ planes of the crystallites [18], as shown in Figure 1, *a*. Next, the porous sample is impregnated with alcohol and subjected to uniaxial compression at a pressure of up to 500 MPa, and then annealed for 30−50h at 830°C. The described procedure leads to texturing of Bi2223 crystallites in a bulk material, as schematically shown in Figure 1, *b*; $a-b$ the crystallite planes are oriented predominantly in the texturing plane (TP in Figure 1, *b*).

Below, the normal to this plane, designated as $\mathbf{N}_{\text{TP}}$, will be used to indicate the mutual orientation of the external field to TP, see Figure 1, *b*. Silver is present in the space between the crystallites in the form of „drops“ with a diameter of $\sim 10-30\,\mu$m (both in porous and textured samples) [18]. The diffraction patterns of the obtained samples contain reflections from the Bi2223 structure and from the BCC

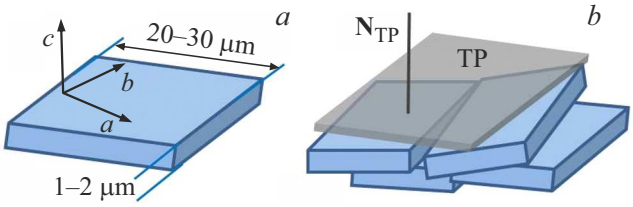

Figure 1. Schematic representation of the arrangement of the crystallographic $a-b$ planes and c axes in a Bi2223 lamellar crystallite (*a*) and Bi2223 crystallites in a textured material (*b*). The plane of preferential orientation of the crystallites is TP (texturing plane) and the normal to it $\mathbf{N}_{\text{TP}}$.

structure of silver. A sample of the composition 70 Vol.% $Bi_{1.8}Pb_{0.3}Sr_{1.9}Ca_2Cu_3O_x$ + 30 Vol.% Ag was studied in this paper.

The temperature of transition to the superconducting state of the sample studied in this paper is ≈ 108 K according to magnetic measurements, and the transition from the state with „zero resistance“ is observed at ≈ 106 K. The density of the critical transport current at $T = 77.4$ K was 220 A/cm^2 (current direction $\mathbf{I} \perp \mathbf{N}_{\text{TP}}$).

2.2. Magnetic measurements

The sample for magnetic measurements was made in the form of a cube oriented along the TP texturing plane with a side length of ≈ 1 mm. Magnetic measurements were performed using LakeShore VSM 8604 magnetometer. All measurements presented in the paper were carried out at a temperature of 78 K. The sample was cooled in a zero external field. Dependencies $M(H)$ were measured using two protocols. A family of private hysteresis loops was measured in the protocol P_1, with a sequential increase in the maximum applied field $\pm H_{\text{max}}$. The step of increasing the maximum field value was ± 2.5 Oe. The hysteresis loop (after cooling in the zero field) was measured in the protocol P_2 to the value of $H_{\text{max}} = \pm 1000$ Oe. The rate of field change for both measurement protocols was ≈ 1 Oe/s. The measurements were carried out in the directions of the external field **H**, perpendicular and parallel to the texturing plane TP. In this case, the magnetic moment of the sample is measured, as standard, along the direction of the external field. The magnetization data are given in electromagnetic units (emu) per gram of sample.

3. Results and discussion

3.1. Anisotropy of magnetic hysteresis from Bi2223 crystallites

Figure 2 shows the dependencies $M(H)$ (protocols P_1, P_2) for $\mathbf{H} \parallel \mathbf{N}_{\text{TP}}$ (Figure 2, *a*) and $\mathbf{H} \perp \mathbf{N}_{\text{TP}}$ (Figure 2, *b*) in the field area up to ± 115 Oe. The upper inserts in Figure 2 illustrate the general view of the dependencies $M(H)$ for the protocols used in the range of field ± 1000 Oe.

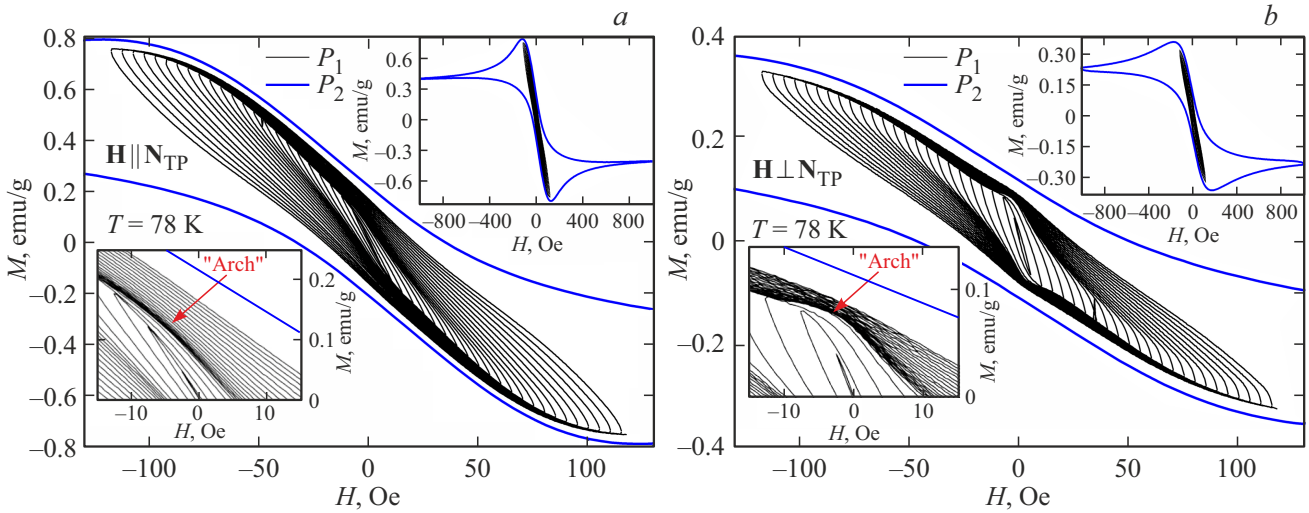

Figure 2. Dependencies $M(H)$, measured using protocols P_1 and P_2 (see section 2.2) for orientations $\mathbf{H} \parallel \mathbf{N}_{TP}$ (a) and $\mathbf{H} \perp \mathbf{N}_{TP}$ (b). Upper inserts show the same in the range of the field ± 1000 Oe. Bottom inserts: behavior of partial hysteresis loops in the vicinity of $H \approx 0$; arrows mark the arc-shaped singularities of the dependencies $M(H)$.

First of all, we would like to note that the magnetization values for the directions $\mathbf{H} \parallel \mathbf{N}_{TP}$ and $\mathbf{H} \perp \mathbf{N}_{TP}$ in the area of fields 100−1000 Oe differ by more than two times.

It is known that Bi2223 single crystals are characterized by a strong anisotropy of magnetization: the value of magnetization M_c can be tens of times higher at $\mathbf{H} \parallel c$ than the magnetization of M_{a-b} at $\mathbf{H} \parallel a-b$ [19]. This difference is much smaller in textured bulk polycrystals Bi2223 [20–24], as can be seen from the data in Figure 2. Obviously, the low anisotropy of textured samples is associated with the effect of disorientation of crystallites [25,26]. For the subsequent analysis of the small hysteresis, it is advisable to show the relative position of the vectors $\mathbf{M}_{a-b}$ and $\mathbf{M}_c$ from an individual Bi2223 crystallite, $a-b$ the plane of which is deflected from the texturing plane TP by a certain angle φ, see Figure 3. If the external field is directed along the texturing plane ($\mathbf{H} \perp \mathbf{N}_{TP}$), then its projections $\mathbf{H}_{a-b}$ onto the plane $a-b$ and $\mathbf{H}_c$ onto the c-axis induce magnetic responses $\mathbf{M}_{a-b}$ and $\mathbf{M}_c$, respectively. In this case, $H_{a-b} = H\cos\varphi$, $H_c = H\sin\varphi$ and ($|\mathbf{M}_c| \gg |\mathbf{M}_{a-b}|$). The fulfillment of the strict inequality $|\mathbf{M}_{c\_H}| > |\mathbf{M}_{a-b\_H}|$ is also logical for the projections of the magnetization $\mathbf{M}_{a-b\_H}$ and $\mathbf{M}_{c\_H}$ on the direction of the external field $\mathbf{H}$.

As a result, in a textured material, even with the orientation $\mathbf{H} \perp \mathbf{N}_{TP}$, the main contribution to the magnetic properties is due to the magnetization of M_c, i.e., shielding currents flowing in it a−b planes of crystallites and trapped Abrikosov vortices (in relatively large fields), located along the axis c. From this consideration, it follows that the effective field H^* will be smaller for $\mathbf{H} \perp \mathbf{N}_{TP}$: $H^* = H\cos\varphi$, where φ is the average misorientation angle of lamellar crystallites relative to the texturing plane [25]. The above explains the rather small anisotropy of the magnitude of the magnetization and the shape of the hysteresis loop for the main („large“) hysteresis of textured Bi2223 (see inserts Figure 2).

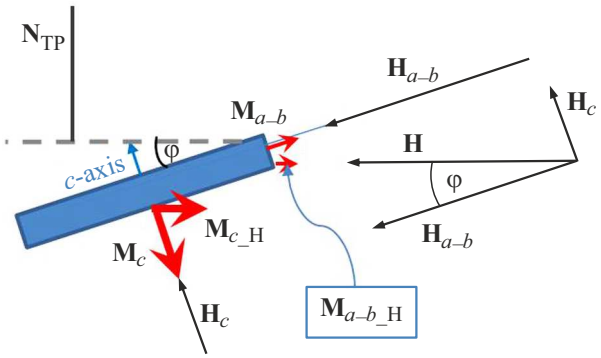

Figure 3. Schematic representation of the effect of the deviation of a single Bi2223 crystallite from the texturing plane on the resulting magnetization. The Bi2223 crystallite (filled rectangle, the crystallographic c-axis is indicated) is deflected from the texturing plane (dashed horizontal line) by angle φ. The resulting magnetization is measured along the external field $\mathbf{H}$. The vectors $\mathbf{H}_{a-b}$ and $\mathbf{H}_c$ are projections $\mathbf{H}$ onto the plane $a-b$ and axis c, magnetization vectors $\mathbf{M}_{a-b}$ and $\mathbf{M}_c$ ($|\mathbf{M}_c| \gg |\mathbf{M}_{a-b}|$) being a diamagnetic response to $\mathbf{H}_{a-b}$ and $\mathbf{H}_c$, as well as projections of these vectors onto the direction of the external field $\mathbf{M}_{a-b\_H}$ and $\mathbf{M}_{c\_H}$.

3.2. Area of existence of small magnetic hysteresis

The data obtained using the protocol P_1 in Figure 2 shows the evolution of the hysteresis loop with an increase in H_{max}. In the protocol P_1, the step to increase the field H_{max} is the same (see section 2.2), however, the distance between the

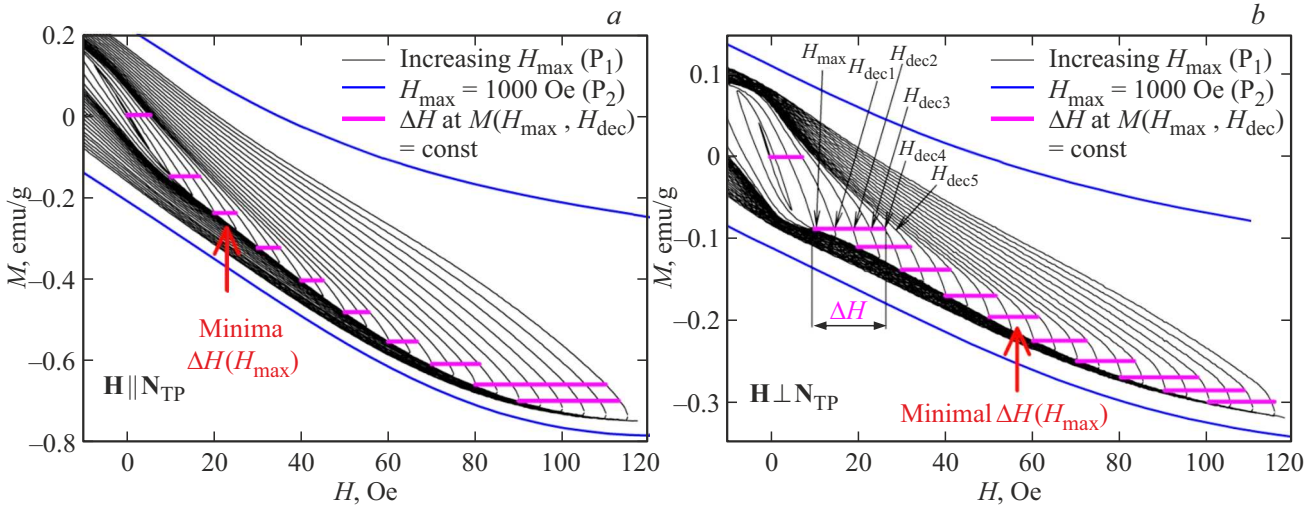

Figure 4. Data from Figure 2 (dependencies $M(H)$) on an enlarged scale. (b) for $H_{max} = 10$ Oe shows an example of determining the hysteresis field width ΔH based on the points H_{dec1}, H_{dec2}, H_{dec3}, H_{dec4}, H_{dec5} shown in the figure. The value ΔH for different values H_{max} corresponds to the length of the horizontal segments; the position of the minimum value ΔH is indicated (see section 3.2).

neighboring branches of the partial hysteresis loops on the coordinate plane M, H is not the same, which is clearly seen when comparing the data in the central region of the coordinate plane and in its other regions. The greatest degree of spatial separation of the partial hysteresis loops is observed in the central region of the coordinate plane, and this behavior suggests the manifestation of a small magnetic hysteresis, which develops in the region of small external fields [15–17]. From a comparison of the data in Figure 2, *a* and *b*, attention is drawn to the different degree of spatial separation of the partial hysteresis loops for orientations $\mathbf{H} \| \mathbf{N}_{TP}$ and $\mathbf{H} \perp \mathbf{N}_{TP}$: for orientations $\mathbf{H} \perp \mathbf{N}_{TP}$ adjacent curves are located further from each other.

A small hysteresis is clearly expressed for granular HTSC of the yttrium system and the bismuth system without texturing in a certain field range — up to $\pm H_{irr1}$ (see Introduction), and the dependence $M(H)$ becomes almost reversible at $H \approx H_{irr1}$ [15–17]. At the same time, the usual „large“ hysteresis from HTSC granules begins to develop already in fields exceeding the values of H_{irr1}. This makes it possible to accurately specify the range of existence of a small magnetic hysteresis and determine the field H_{irr1} [15–17]. There is no area with reversible magnetization behavior in the dependences $M(H)$ in Figure 2 that uniquely determines the field H_{irr1}, which is attributable to the fact that the ranges of small and large hysteresis (from Bi2223 crystallites) overlap. To estimate the value of H_{irr1}, it is advisable to consider the field width of the magnetic hysteresis ΔH (at $M = \text{const}$) and propose a criterion for identifying particular loops of small hysteresis. And it is logical that if the hysteresis width ΔH is minimal for a certain field, then this field will reflect the end of the development of small hysteresis against the background of the development of hysteresis from Bi2223 crystallites.

Figure 4 shows parts of the data in Figure 2 (the range of the field $-10-115$ Oe), and Figure 4, *b* shows an example of determining the hysteresis width ΔH. Let us draw a horizontal line to the right from a point on the coordinate grid at $H = H_{max}$ (for example, at $H_{max} = 10$ Oe), and the intersection points of this line with the nearest branches of the partial hysteresis loops for the decreasing external field H_{dec} are denoted as H_{dec1}, H_{dec2}, H_{dec_i}, see Figure 4, *b*. Next, let us compare the values of the segments $H_{max}H_{dec1}$, $H_{dec1}H_{dec2}$, $H_{dec2}H_{dec3}$, $H_{dec\_i}H_{dec\_i+1}$, etc. The lengths of these segments will be large enough in the area of relatively small fields where the hysteresis branches $M(H_{dec})$ are sparse enough, and this is that very area where a small magnetic hysteresis exists. It can be seen from Figure 4, *b* for $H_{max} = 10$ Oe that the lengths of the segments $H_{max}H_{dec1}$, $H_{dec1}H_{dec2}$, $H_{dec2}H_{dec3}$, $H_{dec3}H_{dec4}$ are approximately the same, and the length of the segment $H_{dec4}H_{dec5}$ is noticeably shorter. This, on a qualitative level, allows assuming that the field width of the small hysteresis ΔH at $H_{max} = 10$ Oe approximately corresponds to the length of the segment $H_{max}H_{dec4}$. We propose the following semi-empirical criterion for determining the width of a small hysteresis ΔH: $\Delta H(H_{max})$ is equal to the value of the segment between H_{max} and H_{dec_i} if the length of the segment $H_{dec\_i}H_{dec\_i+1}$ becomes 85% less than the length of the „previous“ segment $H_{dec\_i\ -1}H_{dec\_i}$.

Using the described algorithm, we obtained the values ΔH for different values H_{max}. The values of ΔH are shown in Figure 4 as horizontal segments, and it can be seen that their length behaves non-monotonously with the growth of H_{max}, which is assumed with the development of magnetic hysteresis from two subsystems (see above). The positions of the minimum value of the hysteresis width are shown in Figure 4. As can be seen from Figure 4, *a, b*, the field at which ΔH is minimal is larger for orientation $\mathbf{H} \perp \mathbf{N}_{TP}$ than

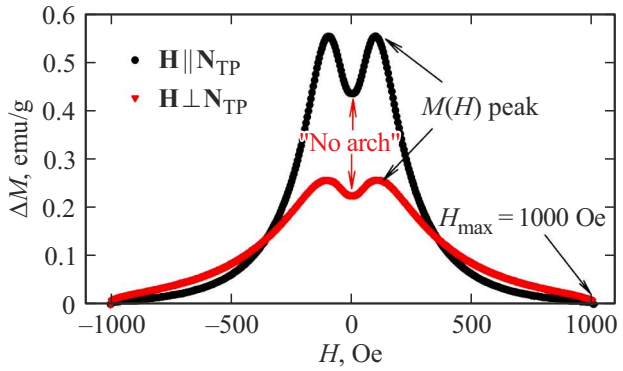

Figure 5. The height of the hysteresis loops $M(H)$ — dependences $\Delta M(H)$ at $H_{max} = 1000$ Oe for orientations $\mathbf{H} \parallel \mathbf{N}_{TP}$ and $\mathbf{H} \perp \mathbf{N}_{TP}$ (from the data of upper insets of Figure 2).

for orientation $\mathbf{H} \parallel \mathbf{N}_{TP}$. Thus, from the data in Figure 4, it can be concluded with confidence that for the studied textured sample, the field range in which a small hysteresis exists is noticeably larger for the orientation $\mathbf{H} \perp \mathbf{N}_{TP}$.

3.3. Arc-shaped singularity on a small magnetic hysteresis loop

A characteristic arch-shaped singularity is visible on specific loops $M(H)$ in Figure 2 in the vicinity of $H \approx 0$, which is highlighted in the lower inserts of Figure 2, *a* and *b*, where the dependences $M(H)$ are shown for positive magnetization values ($M \geq 0$) in the area of field ±15 Oe. It can be seen from a comparison of the data in the lower inserts of Figure 2, *a* and *b*, that for orientation $\mathbf{H} \parallel \mathbf{N}_{TP}$ (Figure 2, *a*) this arch-shaped singularity is expressed weaker than for the orientation $\mathbf{H} \perp \mathbf{N}_{TP}$ (Figure 2, *b*). As was shown earlier [15–17], the arc-shaped singularity of the dependence $M(H)$ in the region of small fields is an „attribute“ of the small hysteresis loop. The disappearance of this arch-shaped singularity at a certain value of H^*_{max} is a sign that the contribution from the subsystem of intergranular boundaries completely disappears in the vicinity of $H \approx 0$ [15]. On the other hand, the degree to which the arch-shaped singularity is pronounced indicates the degree of attenuation of the small hysteresis loop after application of the field H_{max}.

Let us consider the height of the magnetic hysteresis loop $\Delta M(H) = M(H_{dec}) - M(H_{inc})$ (H_{inc} — increasing external field). First, we present the dependencies $\Delta M(H)$ for the field $H_{max} = 1000$ Oe, in which the arch-shaped singularity is no longer observed, see Figure 5. These dependences have maxima (in fields of positive and negative sign), typical for granular superconductors.

The dependencies $\Delta M(H)$ for the sample values H_{max} are shown in Figure 6. The arch-shaped singularity of the dependencies $M(H)$ manifests itself as a peak on the dependencies $\Delta M(H)$, and this is especially noticeable for small values H_{max}. The peak in the vicinity of $H \approx 0$ has the form of a weakly expressed local maximum for the orientation $\mathbf{H} \parallel \mathbf{N}_{TP}$ at $H_{max} = 115$ Oe, and local maxima from the main magnetic hysteresis are also visible (as in Figure 5). Therefore, for the orientation $\mathbf{H} \parallel \mathbf{N}_{TP}$, the characteristic field H^*_{max}, which leads to the disappearance of a small hysteresis, is quite close to the value of 115 Oe. The peak remains sufficiently „sharp“ for the orientation $\mathbf{H} \perp \mathbf{N}_{TP}$ at $H_{max} = 115$ Oe, which indicates that the field H^*_{max} significantly exceeds the value of 115 Oe (maxima from the magnetic hysteresis of Bi2223 crystallites are manifested in a characteristic a form of a „shoulder“).

An unambiguous conclusion follows from the consideration of the evolution of the characteristic arc-shaped singularity of the dependencies $M(H)$ (Figure 2) and the accompanying hysteresis height data $\Delta M(H)$ (Figure 6) that the characteristic field H^*_{max} for the orientation $\mathbf{H} \perp \mathbf{N}_{TP}$ significantly exceeds the field H^*_{max} for orientation $\mathbf{H} \parallel \mathbf{N}_{TP}$.

3.4. Model explaining the anisotropy of small magnetic hysteresis

Based on the results in sections 3.2 and 3.3 it can be said that an anisotropic behavior of small hysteresis is observed in a textured polycrystal based on Bi2223. And if the magnetization values for the main magnetic hysteresis are higher at orientation $\mathbf{H} \parallel \mathbf{N}_{TP}$, then small hysteresis at orientation $\mathbf{H} \perp \mathbf{N}_{TP}$ exists in a significantly larger range of the external field than at orientation $\mathbf{H} \parallel \mathbf{N}_{TP}$. To explain the observed behavior, we consider the specifics of the interaction of subsystems of superconducting granules and intergranular boundaries [15–17], as applied to textured HTSC Bi2223.

Figure 7 shows the directions of magnetic moments from neighboring crystallites (somewhat disaligned relative to the TP plane) in the cases of $\mathbf{H} \parallel \mathbf{N}_{TP}$ (Figure 7, *a*) and $\mathbf{H} \perp \mathbf{N}_{TP}$ (Figure 7, *b*). In the case of $\mathbf{H} \parallel \mathbf{N}_{TP}$, the diamagnetic response of crystallites is determined by the projection of M_c onto the external field of $\mathbf{H}$, i. e., by the vector $\mathbf{M}_{c\_H}$ (contribution from $\mathbf{M}_{a-b}$ negligible). In the case of $\mathbf{H} \perp \mathbf{N}_{TP}$, based on the consideration of Figure 3, it can also be assumed that the diamagnetic response is determined by the vector $\mathbf{M}_{c\_H}$ (the contribution from M_{a-b_H} is significantly less). Magnetic induction lines from vectors $\mathbf{M}_{c\_H}$ are closed through the space between the crystallites, inducing a field $\mathbf{B}_{ind}$ in the intercrystalline boundaries. It can be seen that the fields $\mathbf{B}_{ind}$ induced by neighboring crystallites in the case of $\mathbf{H} \parallel \mathbf{N}_{TP}$ are directed in one direction. However, for the case of $\mathbf{H} \perp \mathbf{N}_{TP}$ (Figure 7, *b*), the vectors $\mathbf{B}_{ind}$ from neighboring crystallites are multidirectional. Obviously, in this case, the influence of the magnetic moments of neighboring crystallites on the induced field in the intercrystalline boundary is partially compensated. Therefore, for the values of the induced field B_{ind} in orientations $\mathbf{H} \parallel \mathbf{N}_{TP}$ and $\mathbf{H} \perp \mathbf{N}_{TP}$, the following inequality can be written:

$$B_{ind}(\mathbf{H} \parallel \mathbf{N}_{TP}) > B_{ind}(\mathbf{H} \perp \mathbf{N}_{TP}). \quad (1)$$

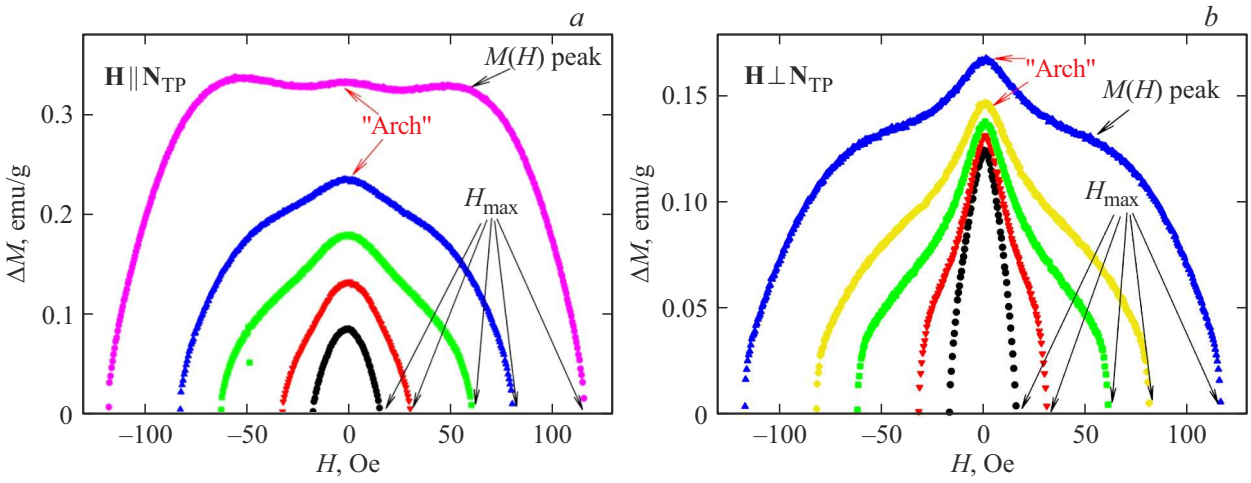

Figure 6. Dependencies $\Delta M(H)$ for different values H_{max} for orientations $\mathbf{H} \parallel \mathbf{N}_{TP}$ (a) and $\mathbf{H} \perp \mathbf{N}_{TP}$ (b). Peaks corresponding to arc-shaped singularitys (see lower inserts in Figure 2) and extremes of dependencies $M(H)$ (upper inserts Figure 2) are marked.

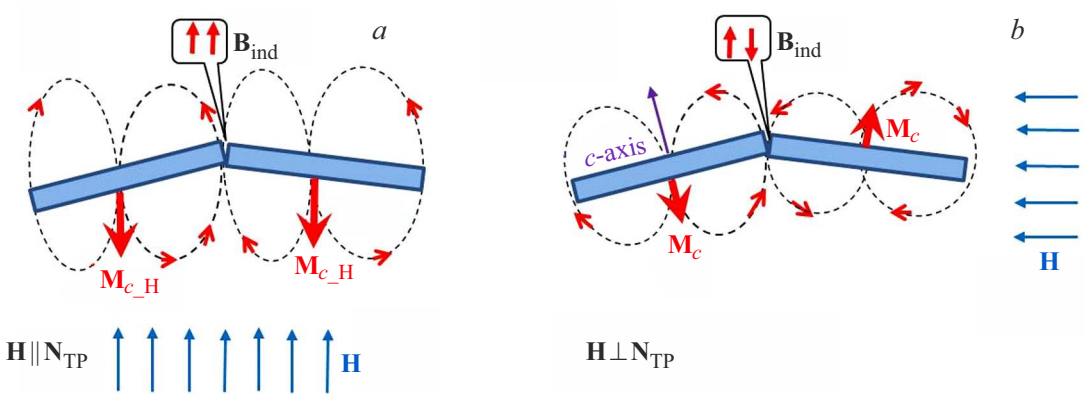

Figure 7. Schematic representation of the directions of magnetic moments $\mathbf{M}_c$, $\mathbf{M}_{c\_H}$ (see Figure 3), magnetic induction lines (dashed lines) induced by them in the space between two neighboring Bi2223 crystallites (rectangles, see Figure 1) in the external field $\mathbf{H}$ for orientations $\mathbf{H} \parallel \mathbf{N}_{TP}$ (a) and $\mathbf{H} \perp \mathbf{N}_{TP}$ (b). The captions schematically show the directions of the induced field $\mathbf{B}_{ind}$ from neighboring crystallites.

In the schematic representation of Figure 7 (also in Figure 3), the case of an increasing field is considered when the resulting magnetization has negative values (diamagnetism). In the case when the external field decreases (under the condition $H \geq 0$), the directions of the magnetic moments $\mathbf{M}_c$, $\mathbf{M}_{c\_H}$, lines of magnetic induction and vectors $\mathbf{B}_{ind}$ are reversed, while the inequality (1) will remain true.

In the area of intercrystalline boundaries, it is appropriate to consider the effective field $\mathbf{B}_{eff}$, which is a superposition of $\mathbf{H}$ and $\mathbf{B}_{ind}$:

$$\mathbf{B}_{eff} = \mathbf{H} + \mathbf{B}_{ind}. \quad (2)$$

It was previously shown that in the expression (2) in the region of small and intermediate fields, the second term dominates due to the compression of the magnetic flux in the intergranular medium [15,27]. It is the field B_{eff} (and not the magnitude of the external field H) that determines the evolution of the small magnetic hysteresis. If the value B_{eff} is large enough, then the response from the subsystem of intercrystalline boundaries becomes vanishingly small. And this situation occurs both in fields of the order H_{irr1} (see above) and in the vicinity of small fields after applying an external field to a certain value H^*_{max}, and then reducing the field (a weakly expressed arc-shaped singularity, see section 3.3). In the latter case, the trapped flux (Abrikosov vortices) in the crystallites induces a field B_{ind} into the intercrystalline boundaries. Due to the inequality (1), the discussed arc-shaped singularity of the dependence $M(H)$ for orientation $\mathbf{H} \parallel \mathbf{N}_{TP}$ disappears with a lower value of the field H^*_{max} (used in the protocol P_1) than for orientation $\mathbf{H} \perp \mathbf{N}_{TP}$.

So, the anisotropy of individual Bi2223 crystallites leads to the fact that the inequality $M(\mathbf{H} \parallel \mathbf{N}_{TP}) > M(\mathbf{H} \perp \mathbf{N}_{TP}$ holds for the main magnetic hysteresis), see inserts Figure 2. At the same time, at the orientation $\mathbf{H} \perp \mathbf{N}_{TP}$, small magnetic hysteresis exists in a larger field range than at the orientation $\mathbf{H} \parallel \mathbf{N}_{TP}$, and this is explained by the influence

of effective fields in the intercrystalline boundaries induced by the magnetic moments of Bi2223 crystallites (Figure 7).

4. Conclusions

For a textured superconducting material based on Bi2223 lamellar crystallites, the orientation of the external field relative to the texturing plane affects the range of the external field in which a small magnetic hysteresis is manifested. When the external field is directed parallel to the texturing plane (parallel to the $a-b$ planes of the crystallites), due to the imperfect orientation of the crystallites, conditions arise under which the influence of the magnetic moments of neighboring crystallites is partially compensated. This leads to the fact that small magnetic hysteresis is manifested in a significantly larger range of external fields than in the orientation when the field is perpendicular to the texturing plane.

Acknowledgments

Magnetic measurements were performed using the equipment of the Krasnoyarsk Regional Center of Research Equipment of Krasnoyarsk Scientific Center, Siberian Branch of the Russian Academy of Sciences.

Funding

The study was performed under the state assignment of the Institute of Physics, Siberian Branch of RAS.

Conflict of interest

The authors declare that they have no conflict of interest.

References

[1] D.J. Resnick, J.C. Garland, J.T. Boyd, S. Shoemaker, R.S. Newrock. Phys. Rev. Lett. **47**, 1542 (1981).
[2] S. Eley, S. Gopalakrishnan, P.M. Goldbart, N. Mason. Nature Physics **8** (1), 59 (2012).
[3] M. Sharma, M. Singh, R.K. Rakshit, S.P. Singh, M. Fretto, N. De Leo, A. Perali, N. Pinto. Nanomaterials, **12**, 4109 (2022).
[4] H. Dersch, G. Blatter. Phys. Rev. B **38** (N16), 11391 (1988).
[5] P. Chaddah, G. Ravi Kumar, A.K. Grover, C. Radhakrishnamurty, G.V.S. Rao. Cryogenics **29**, 907 (1989).
[6] G.E. Gough, M.S. Colclough, D.A. O'Connor, E. Wellhoffer, N.McN. Alford, T.W. Button. Cryogenics **31**, 119 (1991).
[7] J. Jung, M.-K. Mohamed, S.C. Cheng, J.P. Franck. Phys. Rev. B. **42**, 6181 (1990).
[8] I. Edmond, L.D. Firth. J. Phys: Condens. Matter. **4**, 3813 (1992).
[9] S. Senoussi. Journal de Physique III **2** (7), 1041 (1992),
[10] F. Pérez, X. Obradors, J. Fontcuberta, X. Bozec, A. Fert. Supercond. Sci. Technol. **9**, 161 (1996).
[11] B. Andrzejewski, E. Guilmeau, C. Simon. Supercond. Sci. Technol. **14**, 904 (2001).
[12] W.A.C. Passos, P.N. Lisboa-Filho, R. Caparroz, C.C. de Faria, P.C. Venturini, F.M. Araujo-Moreira, S. Sergeenkov, W.A. Ortiz. Physica C **354**, 189 (2001).
[13] D.A. Balaev, A.D. Balaev, S.V. Semenov, D.M. Gokhfeld. Physics of the Solid State **66** (9), 1431 (2024).
[14] E.B. Sonin. JETP Lett. **47** (8), 496 (1988).
[15] D.A. Balaev, S.V. Semenov, D.M. Gokhfeld, M.I. Petrov. JETP **165** (2), 113 (2024).
[16] D.A. Balaev, S.V. Semenov, D.M. Gokhfeld, M.I. Petrov. Physics of the Solid State **66** (4), 506 (2024).
[17] D.A. Balaev, S.V. Semenov, D.M. Gokhfeld, M.I. Petrov. J. Supercond. Nov. Magn. **37**, 1329 (2024).
[18] M.I. Petrov, I.L. Belozerova, K.A. Shaykhutdinov, D.A. Balaev, A.A. Dubrovskii, S.I. Popkov, A.D. Vasilyev, O.N. Mart'yanov. Supercond. Sci. Technol. **21**, 105019 (2008).
[19] N. Clayton, N. Musolino, E. Giannini, V. Garnier, R. Flükiger. Supercond. Sci. Technol. **17**, S563 (2004).
[20] B. Hensel, G. Grasso, R. Flukiger. Phys. Rev. B **51** (N21), 15456 (1995).
[21] G.C. Han. Phys. Rev. B **52** (N2), 1309 (1995).
[22] G.C. Han, C.K. Ong. Phys. Rev. B **56** (N17), 11299 (1997).
[23] D.A. Balaev, S.I. Popkov, S.V. Semenov, A.A. Bykov, K.A. Shaykhutdinov, D.M. Gokhfeld, M.I. Petrov. Physica C **470**, 61 (2010).
[24] D.M. Gokhfeld, D.A. Balaev, S.V. Semenov, M.I. Petrov. Physics of the Solid State **57** (11), 2145 (2015).
[25] D.M. Gokhfeld, D.A. Balaev. Physics of the Solid State **62** (7), 1145 (2020).
[26] D.M. Gokhfeld, S.V. Semenov, M.I. Petrov, I.V. Nemtsev, D.A. Balaev. J. Supercond. Nov. Magn. **36**, 59 (2023).
[27] S.V. Semenov, A.D. Balaev, D.A. Balaev. J. Appl. Phys. **125**, 033903 (2019).

Translated by A.Akhtyamov